AIMS Mathematics, 11(5): 13937–13962.
DOI:10.3934/math.2026573
Received: 26 February 2026
Revised: 13 April 2026
Accepted: 17 April 2026
Published: 18 May 2026

https://www.aimspress.com/journal/Math

Research article

Topological invariants of sustainable network for energy efficiency and environmental impact reduction

Jun Yang[1], Hifza Iqbal[2,*], Muhammad Akmal[2] and Muhammad Akhtar Tarar[3]

[1] School of Economics and Law, Chaohu University, Chaohu, China
[2] Department of Mathematics and Statistics, The University of Lahore, Defence Road Campus, Lahore, Pakistan.
[3] Department of Civil Engineering, The University of Lahore, Defence Road Campus, Lahore, Pakistan

* **Correspondence:** Email: iqbalhifza3@gmail.com.

Abstract: In this work, we employ a graph-theoretical framework to study the structural characteristics of nanocarbon sheets. Key auxiliary properties are predicted using the Van, R, and S topological indices, which makes it easier to design materials that are both energy-efficient and environmentally friendly. The analysis assesses how topological characteristics can affect performance metrics that are important for long-term uses in green energy systems. Our results show how useful these descriptors are for simulating the behavior of sustainable nanomaterials based on nanocarbons and directing the creation of devices with lower power consumption and higher energy efficiency. Theoretical expressions are clearly visualized by the use of tables and three-dimensional MATLAB figures.

Keywords: sustainable network; topological index; nanostructure
Mathematics Subject Classification: 05C02, 05C90

1. Introduction

Chemical graph theory is a branch of mathematical chemistry that applies graph theory to the mathematical description of chemical and organic phenomena [1]. By using graphs to illustrate molecular structures where atoms are represented by vertices and chemical bonds by edges, this field establishes a close connection between chemistry and graph theory a very helpful tool for resolving challenging molecular issues is chemical graph theory. The chemical sciences, including materials research, medicinal design, and structural chemistry, have made extensive use of it [2]. Quantitative structure activity relationship (QSAR) and quantitative structure property relationship (QSPR) are two

techniques used in cheminformatics, a field that blends chemistry and information science to predict how chemicals will behave in living organisms and interact with one another [3]. Molecular graphs are a major component of these studies, and the data they provide are crucial for connecting structure to observable characteristics. The composition of a molecule is depicted by a graph G in chemical graph theory. Several graph metrics are used by entropy-based approaches to gather structural data. The structure of complex networks and chemical graphs serves as the foundation for these techniques.

Graph entropy measurements convert molecular graph data into information theory-based metrics [4]. The peculiar physical, chemical, and electrical characteristics have made nanostructures, particularly carbon nanosheets, a frequent subject of recent news. These two-dimensional materials have a large surface area relative to their volume, are incredibly strong, and conduct electricity well. They would therefore be ideal for energy storage devices, sensors, nanoelectronics, and catalysis [5,6].

In order to comprehend the complex structural characteristics of rapidly developing carbon-based nanomaterials, researchers are investigating mathematical methods. We can model and predict the properties of nanostructures with a solid theoretical foundation provided by mathematical chemistry. One of the most crucial tools in this field is graph theory, which enables us to study complex molecular systems by converting them into mathematical objects. By employing topological descriptors, graph theoretic modeling enables researchers to systematically examine nanoscale materials such as carbon nanosheets [7, 8].

Topological indices are numerical values derived from a graph that illustrates the molecular structure. Guessing the chemical, physical, and biological characteristics of materials and molecules is a common use for them. These indices contain structural information about bonding configurations, connection patterns, and vertex degrees [9, 10]. We examine four- and eight-membered carbon nanosheets represented as $T^1C_4C_8(S)[p,q]$. Graph theoretic analysis benefits from the intricate structure of these sheets [11].

To better understand increasingly complex nanostructures, numerous degree-based topological indices have been proposed in recent years. For identifying subtle variations in the connections between molecules, the Van, R, and S indices have been demonstrated to be useful instruments [12, 13]. These indices, which examine the interactions between vertex degrees, have been strongly connected to the physicochemical and thermodynamic characteristics of chemical networks. Among the degree-based descriptors that have been studied the most are Randic type indices. They have been successfully used on graphene and nanotubes, among other carbon nanostructures [14, 15]. They are far more effective for large nanosheets due to their generalizations and inversions. Complex chemical graphs can be effectively characterized using Van indices, which were created to measure the strength of vertex interactions [16, 17]. Another significant type of structural descriptor that examines the effects of higher-order connectivity are the S indices. When separating nanomaterials with similar structures, these indices are highly helpful.

Additionally, they have been effectively employed in research using entropy as a metric [18, 19]. When paired with information-theoretic concepts, S indices help us to comprehend the complexity and stability of molecular systems. According to recent studies, carbon nanostructures can be studied using Van, R, and S indices in conjunction with entropy metrics [20, 21]. Recent years have seen a major increase in interest in the statistical and structural characteristics of complex networks, especially when considering fractal-based models. Similarly, authors in [22] investigated a class of fractal networks, topological properties, and carried out a thorough statistical analysis.

The information content and structural disorder are fully depicted by these techniques, which are crucial for forecasting the behavior of materials at the nanoscale. Classic carbon nanostructures have been extensively studied, but mixed C_4 and C_8 cycle carbon nanosheets using Van, R, and S indices have received less attention. Research in this area has been limited, highlighting the significance of conducting systematic studies on the index behavior and closed-form expressions of these nanosheets [23–25]. This work attempts to remove the research gap by offering a comprehensive analysis of the Van, R, and S topological indices for $T^1C_4C_8(S)[p, q]$ carbon nanosheets. We hope to improve our understanding of the fundamental structural characteristics of carbon nanosheets and their implications for useful applications in materials science and nanotechnology by examining these indices [26–29]. This study makes it easier to continue improving mathematical models for sophisticated carbon-based materials.

Graph-theoretical techniques have broad applicability beyond nanomaterials, including urban planning optimization [30,31], medicinal chemistry [32–36], and molecular structure analysis [37,38]. This underscores the versatility of topological descriptors in modeling complex systems across diverse domains. Experimental validation is required to quantify correlations between index values and physical properties, like conductivity and mechanical strength, even though the study offers predictive insights based on topological descriptors.

The Van, R, and S indices, predictive power makes it possible to find nanocarbon configurations that reduce energy usage. These techniques can indirectly lessen the environmental impact of nanodevices and related applications by directing the design of energy-efficient materials. Our study develops a theoretical framework based on topological descriptors that can direct the optimization of nanocarbon structures in terms of structural performance and energy efficiency. By offering a thorough analytical framework, as well as numerical and graphical validation, this study seeks to close the gap. Energy storage systems, nanoelectronic devices, and catalytic processes are examples of green energy applications that directly benefit from these features. These materials are crucial for improving performance and lowering energy consumption in sustainable technologies.

2. Basic definitions

A graph $G = (V, E)$ is made up of two sets, β and E, that are not empty. We refer to the components of β as vertices and those of E as edges. The degree of a vertex β, which is written as $\deg(\beta)$, is the total number of edges that pass through it. The open neighborhood of β is the set of all vertices that share an edge with it. It is denoted by N_β. Some basic concepts and formulas are given in Table 1, [39].

Table 1. Graph-theoretic definitions and indices.

Definition	Notation	Formula/Description
Degree of Vertex	$\deg(\beta)$	Number of edges incident to vertex β
Open Neighborhood	N_β	Set of all adjacent vertices to β
Sum Degree	S_β	$\sum_{\alpha\in N_\beta} \deg(\alpha)$
Multiplication Degree	M_β	$\prod_{\alpha\in N_\beta} \deg(\alpha)$
Van Degree	$\text{van}(\beta)$	$\frac{S_\beta}{M_\beta}$
Reverse Van Degree	$\text{rvan}(\beta)$	$\frac{M_\beta}{S_\beta}$
R Degree	$r(\beta)$	$M_\beta + S_\beta$
Reverse R Degree	$rr(\beta)$	$\frac{1}{M_\beta + S_\beta}$
S Degree	$s(\beta)$	$\lvert M_\beta - S_\beta\rvert$
First Van Index	$\text{Van}_1(G)$	$\sum_{\alpha\in V(G)} \text{van}(\alpha)$
Second Van Index	$\text{Van}_2(G)$	$\sum_{\alpha,\beta\in E(G)} \text{van}(\alpha)\text{van}(\beta)$
Third Van Index	$\text{Van}_3(G)$	$\sum_{\alpha,\beta\in E(G)} [\text{van}(\alpha) + \text{van}(\beta)]$
First Reverse Van Index	$\text{Van}_1^r(G)$	$\sum_{\beta\in V(G)} \text{rvan}(\beta)$
Second Reverse Van Index	$\text{Van}_2^r(G)$	$\sum_{\alpha,\beta\in E(G)} \text{rvan}(\alpha)\text{rvan}(\beta)$
Third Reverse Van Index	$\text{Van}_3^r(G)$	$\sum_{\alpha,\beta\in E(G)} [\text{rvan}(\alpha) + \text{rvan}(\beta)]$
First R Index	$R_1(G)$	$\sum_{\beta\in V(G)} r(\beta)$
Second R Index	$R_2(G)$	$\sum_{\alpha,\beta\in E(G)} r(\alpha)r(\beta)$
Third R Index	$R_3(G)$	$\sum_{\alpha,\beta\in E(G)} [r(\alpha) + r(\beta)]$
First Reverse R Index	$R_1^r(G)$	$\sum_{\beta\in V(G)} rr(\beta)$
Second Reverse R Index	$R_2^r(G)$	$\sum_{\alpha,\beta\in E(G)} rr(\alpha)rr(\beta)$
Third Reverse R Index	$R_3^r(G)$	$\sum_{\alpha,\beta\in E(G)} [rr(\alpha) + rr(\beta)]$
First S Index	$S_1(G)$	$\sum_{\beta\in V(G)} s(\beta)$
Second S Index	$S_2(G)$	$\sum_{\alpha,\beta\in E(G)} s(\alpha)s(\beta)$
Third S Index	$S_3(G)$	$\sum_{\alpha,\beta\in E(G)} [s(\alpha) + s(\beta)]$

3. Results

Nanosheet $T^1C_4C_8(S)[p,q]$ is a two dimensional structure made up of alternating tetragonal (C_4) and octagonal (C_8) units. It is possible to make this nanosheet by putting C_4 and C_8 in a certain trivalent pattern. The nanosheet structure is shown in Figure 1 and numbers p and q tell you how many octagonal units are in each row and column. This nanosheet has $8pq$ vertices and $12pq - 2(p + q)$ edges. Tables 2 and 3 show their respective counts.

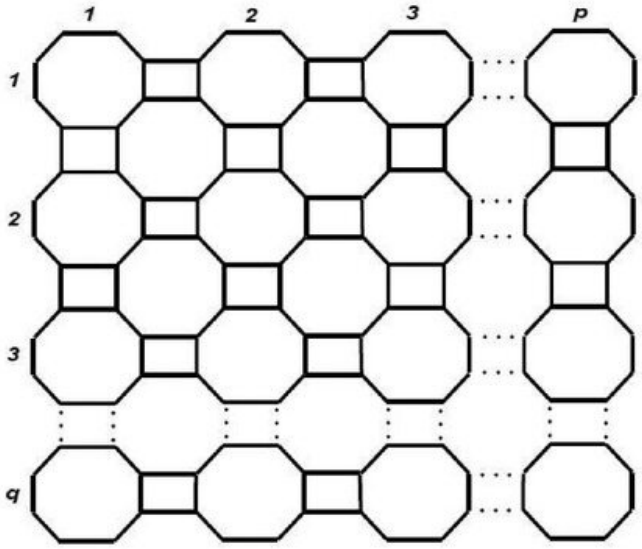

Figure 1. $T^1C_4C_8(S)[p,q]$.

Table 2. Vertex partition for $T^1C_4C_8(S)[p,q]$.

deg(u)	Number of vertices	Set of vertices
2	$4p + 4q$	V_1
3	$8pq - 4(p + q)$	V_2

Table 3. Edge partition for $T^1C_4C_8(S)[p,q]$.

deg$u$,degβ	Number of edges	Set of edges
(2,2)	$2p + 2q + 4$	E_1
(3,2)	$4p + 4q - 8$	E_2
(3,3)	$12pq - 8(p + q) + 4$	E_3

Theorem 1. *The first Van index of $T^1C_4C_8(S)[p,q]$ is given by*

$$Van_1(T^1) = \frac{1}{9}\left(8pq + \frac{217}{9}(p + q) + \frac{142}{9}\right).$$

Proof. By using the definition of the first Van index defined in Table 1 and information from Table 4, the first van index of $T^1C_4C_8(S)[p,q]$ is

Table 4. Van degree table for $T^1C_4C_8(S)[p,q]$.

vanβ	Number of vertices
1	8
$\frac{5}{6}$	$4p+4q-8$
$\frac{4}{9}$	$4p+4q-8$
$\frac{1}{3}$	$8pq-8(p+q)+8$

$$\begin{aligned} Van_1(T^1) &= \sum_{\alpha\in V(G)} \text{van}(\alpha)^2, \\ &= 8(1)^2+(4p+4q-8)\left(\frac{5}{6}\right)^2+(4p+4q-8)\left(\frac{4}{9}\right)^2+(8pq-8p-8q+8)\left(\frac{1}{3}\right)^2. \end{aligned}$$

After simplification, the value of the first Van index for $T^1C_4C_8(S)[p,q]$ is obtained as

$$\text{Van}_1(T^1) = \frac{1}{9}\left(8pq+\frac{217}{9}(p+q)+\frac{142}{9}\right).$$

□

Theorem 2. *The second Van index of $T^1C_4C_8(S)[p,q]$ is given as*

$$Van_2(T^1) = \frac{12}{9}pq+\frac{481}{162}(p+q)+\frac{86}{81}.$$

Proof. By using the definition of the second Van index defined in Table 1 and information from Table 5, the second Van index of $T^1C_4C_8(S)[p,q]$ is

Table 5. Van degrees of end vertices of edges for $T^1C_4C_8(S)[p,q]$.

(van(α), van(β))	Number of edges
(1,1)	4
$(1,\frac{5}{6})$	8
$(\frac{5}{6},\frac{5}{6})$	$2p+2q-8$
$(\frac{5}{6},\frac{4}{9})$	$4p+4q-8$
$(\frac{4}{9},\frac{4}{9})$	$2p+2q-4$
$(\frac{4}{9},\frac{1}{3})$	$4p+4q-8$
$(\frac{1}{3},\frac{1}{3})$	$12pq-8(p+q)+8$

$$\begin{aligned} \text{Van}_2(T^1) &= \sum_{\alpha,\beta\in E(G)} \text{van}(\alpha)\times\text{van}(\beta), \\ &= 4+\frac{40}{6}+\frac{50}{36}p+\frac{50}{36}q-\frac{200}{36}+\frac{80}{54}p+\frac{80}{54}q-\frac{160}{54}+\frac{32}{81}p+\frac{32}{81}q \\ &\quad -\frac{64}{81}+\frac{16}{27}p+\frac{16}{27}q-\frac{32}{27}+\frac{12}{9}pq-\frac{8}{9}p-\frac{9}{9}q+\frac{8}{9}. \end{aligned}$$

After simplification, the value of the second Van index for $T^1C_4C_8(S)[p,q]$ is obtained as

$$\text{Van}_2(T^1) = \frac{12}{9}pq + \frac{481}{162}(p+q) + \frac{86}{81}.$$

□

Theorem 3. *The third Van index of $T^1C_4C_8(S)[p,q]$ is given as*

$$Van_3(T^1) = \frac{24}{3}pq + \frac{34}{3}(p+q) - \frac{16}{3}.$$

Proof. By using the definition of the third Van index defined in Table 1 and information from Table 5, the third Van index of $T^1C_4C_8(S)[p,q]$ is

$$\begin{aligned}\text{Van}_3(T^1) &= \sum_{v\in V(G)} [\text{van}(\alpha) + \text{van}(\beta)],\\ &= 8 + \frac{88}{6} + \frac{20}{6}p + \frac{20}{6}q - \frac{80}{6} + \frac{92}{18}p + \frac{92}{18}q - \frac{184}{18} + \frac{16}{9}p + \frac{16}{9}q\\ &\quad -\frac{32}{9} + \frac{28}{9}p + \frac{28}{9}q - \frac{56}{9} + \frac{24}{3}pq - \frac{16}{3}p - \frac{16}{3}q + \frac{16}{3}.\end{aligned}$$

After simplification, the value of the third Van index for $T^1C_4C_8(S)[p,q]$ is obtained as

$$\text{Van}_3(T^1) = \frac{24}{3}pq + \frac{34}{3}(p+q) - \frac{16}{3}.$$

□

Theorem 4. *The first reverse Van index of $T^1C_4C_8(S)[p,q]$ is given by*

$$Van_r^1(T^1) = 72pq - \frac{4599}{100}(p+q) + \frac{1399}{50}.$$

Proof. By using the definition of the first reverse Van index defined in Table 1 and information from Table 6, the first reverse Van index of $T^1C_4C_8(S)[p,q]$ is

Table 6. Reverse Van degree table for $T^1C_4C_8(S)[p,q]$.

rvan(β)	Number of vertices
1	8
$\frac{6}{5}$	$4p+4q-8$
$\frac{9}{4}$	$4p+4q-8$
$\frac{3}{1}$	$8pq-8(p+q)+8$

$$\begin{aligned}\text{Van}_r^1(T^1) &= \sum_{\beta\in V(G)} \text{rvan}(\beta),\\ &= 8(1)^2 + (4p+4q-8)\left(\frac{6}{5}\right)^2 + (4p+4q-8)\left(\frac{9}{4}\right)^2\end{aligned}$$

$$+(8pq - 8p - 8q + 8)\left(\frac{3}{1}\right)^2.$$

After simplification, the value of the first reverse Van index for $T^1C_4C_8(S)[p, q]$ is obtained as

$$\text{Van}_r^1(T^1) = 72pq - \frac{4599}{100}(p + q) + \frac{1399}{50}.$$

□

Theorem 5. *The second reverse Van index of $T^1C_4C_8(S)[p, q]$ is given by*

$$Van_r^2(T^1) = 108pq - \frac{4239}{200}(p + q) - \frac{1537}{100}.$$

Proof. By using the definition of the second reverse Van index defined in Table 1 and information from Table 7, we define the second reverse Van index $T^1C_4C_8(S)[p, q]$ is

Table 7. Reverse Van degrees of end vertices of edges for $T^1C_4C_8(S)[p, q]$.

(rvan(α), rvan(β))	Number of edges
$(1, 1)$	4
$\left(1, \frac{6}{5}\right)$	8
$\left(\frac{6}{5}, \frac{6}{5}\right)$	$2p + 2q - 8$
$\left(\frac{6}{5}, \frac{9}{4}\right)$	$4p + 4q - 8$
$\left(\frac{9}{4}, \frac{9}{4}\right)$	$2p + 2q - 4$
$\left(\frac{9}{4}, \frac{3}{1}\right)$	$4p + 4q - 8$
$\left(\frac{3}{1}, \frac{3}{1}\right)$	$12pq - 8(p + q) + 8$

$$\begin{aligned}\text{Van}_r^2(T^1) &= \sum_{\alpha,\beta\in E(G)} \text{rvan}(\alpha) \times \text{rvan}(\beta),\\ &= 4 + \frac{48}{3} + \frac{72}{25}p + \frac{72}{25}q - \frac{288}{25} + \frac{216}{20}p + \frac{216}{20}q - \frac{432}{20} + \frac{162}{16}p\\ &\quad + \frac{162}{16}q - \frac{324}{16} + \frac{108}{4}p + \frac{108}{4}q - \frac{216}{4} + 108pq - 72p + 72.\end{aligned}$$

After simplification, the value of the second reverse Van index for $T^1C_4C_8(S)[p, q]$ is obtained as

$$\text{Van}_r^2(T^1) = 108pq - \frac{4239}{200}(p + q) - \frac{1537}{100}.$$

□

Theorem 6. *The third reverse Van index of $T^1C_4C_8(S)[p, q]$ is given by*

$$Van_r^3(T^1) = 72pq - \frac{112}{5}(p + q) - \frac{118}{5}.$$

Proof. By using the definition of the third reverse Van index defined in Table 1 and information from Table 7, the third reverse Van index $T^1C_4C_8(S)[p,q]$ is

$$\begin{aligned}\mathrm{Van}_r^3(T^1) &= \sum_{\alpha,\beta\in E(G)} \mathrm{rvan}(\alpha)+\mathrm{rvan}(\beta),\\ &= 8+\frac{88}{5}+\frac{24}{5}p+\frac{24}{5}q-\frac{96}{10}+\frac{276}{20}p+\frac{276}{20}q-\frac{552}{20}+\frac{36}{4}p+\frac{36}{4}q-\frac{72}{4}\\ &\quad +\frac{88}{4}p+\frac{88}{4}q-\frac{168}{4}+72pq-72p-72q+48.\end{aligned}$$

After simplification, the value of the third reverse Van index for $T^1C_4C_8(S)[p,q]$ is obtained as

$$\mathrm{Van}_r^3(T^1) = 72pq-\frac{112}{5}(p+q)-\frac{118}{5}.$$

□

Theorem 7. *The first r index of $T^1C_4C_8(S)[p,q]$ is given by*

$$R_1(T^1) = 10368pq-7180(p+q)+4504.$$

Proof. By using the definition of the first r index defined in Table 1 and information from Table 8, the first r index of $T^1C_4C_8(S)[p,q]$ is

Table 8. R degree r(β) partition for vertices of $T^1C_4C_8(S)[p,q]$.

r(β)	Number of vertices
8	8
11	$4p+4q-8$
26	$4p+4q-8$
36	$8pq-8(p+q)+8$

$$\begin{aligned}\mathrm{R}_1(T^1) &= \sum_{\beta\in V(G)} \mathrm{r}(\beta)^2,\\ &= 8(8)^2+(4p+4q-8)(11)^2+(4p+4q-8)(26)^2+(8pq-8p-8q+8)(36)^2.\end{aligned}$$

After simplification, the value of the first r index for $T^1C_4C_8(S)[p,q]$ is obtained as

$$\mathrm{R}_1(T^1) = 10368pq-7180(p+q)+4504.$$

□

Theorem 8. *The second r index of $T^1C_4C_8(S)[p,q]$ is given by*

$$R_2(T^1) = 15552pq-3886(p+q)-1800.$$

Proof. By using the definition of the second r index defined in Table 1 and information from Table 9, the second r index of $T^1C_4C_8(S)[p,q]$ is

Table 9. R degrees of end vertices of edges for $T^1C_4C_8(S)[p,q]$.

(r(α), r(β))	Number of edges
(8, 18)	4
(8, 11)	8
(11, 11)	$2p + 2q - 8$
(11, 26)	$4p + 4q - 8$
(26, 26)	$2p + 2q - 4$
(26, 36)	$4p + 4q - 8$
(36, 36)	$12pq - 8(p + q) + 8$

$$\begin{aligned} \mathrm{R}_2(T^1) &= \sum_{\alpha,\beta\in E(G)} \mathrm{r}(\alpha)\times r(\beta), \\ &= 4(18\times 8) + 8(11\times 8) + (2p + 2q - 8)(11\times 11) + (4p + 4q - 8)(11\times 26) \\ &\quad +(2p + 2q - 4)(26\times 26) + (4p + 4q - 8)(26\times 36) + (12pq - 8p - 8q + 8) \\ &\quad (36\times 36). \end{aligned}$$

After simplification, the value of the second r index for $T^1C_4C_8(S)[p,q]$ is obtained as

$$\mathrm{R}_2(T^1) = 15552pq - 3886(p + q) - 1800.$$

□

Theorem 9. *The third r index of $T^1C_4C_8(S)[p,q]$ is given by*

$$R_3(T^1) = 864pq - 32(p + q) - 344.$$

Proof. By using the definition of the third r index defined in Table 1 and information from Table 9, the third r index of $T^1C_4C_8(S)[p,q]$ is

$$\begin{aligned} \mathrm{R}_3(T^1) &= \sum_{\alpha,\beta\in E(G)} \mathrm{r}(\alpha) + \mathrm{r}(\beta), \\ &= 4(18 + 8) + 8(11 + 8) + (2p + 2q - 8)(11 + 11) + (4p + 4q - 8)(11 + 26) \\ &\quad +(2p + 2q - 4)(26 + 26) + (4p + 4q - 8)(26 + 36) + (12pq - 8p - 8q + 8) \\ &\quad (36 + 36). \end{aligned}$$

After simplification, the value of the third r index for $T^1C_4C_8(S)[p,q]$ is obtained as

$$\mathrm{R}_3(T^1) = 864pq - 32(p + q) - 344.$$

□

Theorem 10. *The first reverse r index of $T^1C_4C_8(S)[p,q]$ is given by*

$$R_r^1(T^1) = \frac{8}{1296}pq + \frac{108665}{312738}(p+q) + \frac{705253}{13250952}.$$

Proof. By using the definition of the first reverse r index defined in Table 1 and information from Table 10, the first reverse r index of $T^1C_4C_8(S)[p,q]$ is

Table 10. Reverse r degree rr(β) partition for vertices of $T^1C_4C_8(S)[p,q]$.

rr(β)	Number of vertices
$\frac{1}{8}$	8
$\frac{1}{11}$	$4p+4q-8$
$\frac{1}{26}$	$4p+4q-8$
$\frac{1}{36}$	$8pq-8(p+q)+8$

$$\begin{aligned} \mathrm{R}_r^1(T^1) &= \sum_{\beta\in V(G)} \mathrm{rr}(\beta)^2, \\ &= 8(\frac{1}{8})^2 + (4p+4q-8)(\frac{1}{11})^2 + (4p+4q-8)(\frac{1}{26})^2 \\ &\quad +(8pq-8p-8q+8)(\frac{1}{36})^2. \end{aligned}$$

After simplification, the value of the first reverse r index for $T^1C_4C_8(S)[p,q]$ is obtained as

$$\mathrm{R}_r^1(T^1) = \frac{8}{1296}pq + \frac{108665}{312738}(p+q) + \frac{705253}{13250952}.$$

□

Theorem 11. *The second reverse r index of $T^1C_4C_8(S)[p,q]$ is given by*

$$R_r^2(T^1) = \frac{12}{1296}pq + \frac{103813}{2208492}(p+q) + \frac{1352393}{26501904}.$$

Proof. By using the definition of the second reverse r index defined in Table 1 and information from Table 11, the second reverse r index of $T^1C_4C_8(S)[p,q]$ is

Table 11. Reverse r degrees of end vertices of edges for $T^1C_4C_8(S)[p,q]$.

(rr(α), rr(β))	Number of edges
$\left(\frac{1}{8},\frac{1}{8}\right)$	4
$\left(\frac{1}{8},\frac{1}{11}\right)$	8
$\left(\frac{1}{11},\frac{1}{11}\right)$	$2p+2q-8$
$\left(\frac{1}{11},\frac{1}{26}\right)$	$4p+4q-8$
$\left(\frac{1}{26},\frac{1}{26}\right)$	$2p+2q-4$
$\left(\frac{1}{26},\frac{1}{36}\right)$	$4p+4q-8$
$\left(\frac{1}{36},\frac{1}{36}\right)$	$12pq-8(p+q)+8$

$$\begin{aligned}
\mathrm{R}_r^2(T^1) &= \sum_{\alpha,\beta\in E(G)} \mathrm{rr}(\alpha)\times rr(\beta),\\
&= 4(\frac{1}{8}\times\frac{1}{8})+8(\frac{1}{8}\times\frac{1}{11})+(2p+2q-8)(\frac{1}{11}\times\frac{1}{11})\\
&\quad +(4p+4q-8)(\frac{1}{11}\times\frac{1}{26})+(2p+2q-4)(\frac{1}{26}\times\frac{1}{26})+(4p+4q-8)\\
&\quad (\frac{1}{26}\times\frac{1}{36})+(12pq-8p-8q+8)(\frac{1}{36}\times\frac{1}{36}).
\end{aligned}$$

After simplification, the value of the second reverse r index for $T^1C_4C_8(S)[p,q]$ is obtained as

$$\mathrm{R}_r^2(T^1)=\frac{12}{1296}pq+\frac{103813}{2208492}(p+q)+\frac{1352393}{26501904}.$$

□

Theorem 12. *The third reverse r index of $T^1C_4C_8(S)[p,q]$ is given by*

$$R_r^3(T^1) = \frac{2}{3}pq+\frac{367}{429}(p+q)-\frac{200}{1287}.$$

Proof. By using the definition of the third reverse r index defined in Table 1 and information from Table 11, the third reverse r index of $T^1C_4C_8(S)[p,q]$ is

$$\begin{aligned}
\mathrm{R}_r^3(T^1) &= \sum_{\alpha,\beta\in E(G)} [rr(\alpha)+rr(\beta)],\\
&= 4(\frac{1}{8}+\frac{1}{8})+8(\frac{1}{8}+\frac{1}{11})+(2p+2q-8)(\frac{1}{11}+\frac{1}{11})+(4p+4q-8)(\frac{1}{11}+\frac{1}{26})\\
&\quad +(2p+2q-4)(\frac{1}{26}+\frac{1}{26})+(4p+4q-8)(\frac{1}{26}+\frac{1}{36})+(12pq-8p-8q+8)\\
&\quad (\frac{1}{36}+\frac{1}{36}).
\end{aligned}$$

After simplification, the value of the third reverse r index for $T^1C_4C_8(S)[p,q]$ is obtained as

$$\mathrm{R}_r^3(T^1) = \frac{2}{3}pq+\frac{367}{429}(p+q)-\frac{200}{1287}.$$

□

Theorem 13. *The first s index of $T^1C_4C_8(S)[p,q]$ is given by*

$$S_1(T^1) = 2592pq-2188(p+q)+1784.$$

Proof. By using the definition of the first s index defined in Table 1 and information from Table 12, the first s index of $T^1C_4C_8(S)[p,q]$ is

Table 12. S degree s(β) partition for vertices of $T^1C_4C_8(S)[p,q]$.

s(β)	Number of vertices
0	8
1	$4p+4q-8$
10	$4p+4q-8$
18	$8pq-8(p+q)+8$

$$\begin{aligned} \mathrm{S}_1(T^1) &= \sum_{\beta\in V(G)} \mathrm{s}(\beta)^2, \\ &= 8(0)^2+(4p+4q-8)(1)^2+(4p+4q-8)(10)^2+(8pq-8p-8q+8)(18)^2. \end{aligned}$$

After simplification, the value of the first s index for $T^1C_4C_8(S)[p,q]$ is obtained as

$$\mathrm{S}_1(T^1) = 2592pq-2188(p+q)+1784.$$

□

Theorem 14. *The second s index of $T^1C_4C_8(S)[p,q]$ is given by*

$$S_2(T^1) = 3888pq-1630(p+q)+64.$$

Proof. By using the definition of the second s index defined in Table 1 and information from Table 13, the second s index of $T^1C_4C_8(S)[p,q]$ is

Table 13. S degree table for end vertices of $T^1C_4C_8(S)[p,q]$.

(s(α), s(β))	Number of edges
(0, 0)	4
(0, 1)	8
(1, 1)	$2p+2q-8$
(1, 10)	$4p+4q-8$
(10, 10)	$2p+2q-4$
(10, 18)	$4p+4q-8$
(18, 18)	$12pq-8(p+q)+8$

$$\begin{aligned} \mathrm{S}_2(T^1) &= \sum_{\alpha\beta\in E(G)} \mathrm{s}(\alpha)\times s(\beta), \\ &= 4(0\times 0)+8(0\times 1)+(2p+2q-8)(1\times 1)+(4p+4q-8)(1\times 10) \\ &\quad +(2p+2q-4)(10\times 10)+(4p+4q-8)(10\times 18)+(12pq-8p-8q+8) \\ &\quad (18\times 18). \end{aligned}$$

After simplification, the value of the second s index for $T^1C_4C_8(S)[p,q]$ is obtained as

$$\mathrm{S}_2(T^1) = 3888pq-1630(p+q)+64.$$

□

Theorem 15. *The third s index of $T^1C_4C_8(S)[p,q]$ is given by*

$$S_3(T^1) = 432pq - 88(p+q) - 122.$$

Proof. By using the definition of the third s index defined in Table 1 and information from Table 13, the third s index of $T^1C_4C_8(S)[p,q]$ is

$$\begin{aligned} \mathrm{R}_3(T^1) &= \sum_{\alpha\beta\in E(G)} [r(\alpha)+r(\beta)], \\ &= 4(0+0)+8(0+1)+(2p+2q-8)(1+1)+(4p+4q-8)(1+10) \\ &\quad +(2p+2q-4)(10+10)+(4p+4q-8)(10+18) \\ &\quad +(12pq-8p-8q+8)(18+18). \end{aligned}$$

After simplification, the value of the third s index for $T^1C_4C_8(S)[p,q]$ is obtained as

$$\mathrm{S}_3(T^1) = 432pq - 88(p+q) - 122.$$

□

4. Discussion

The obtained results show that for the carbon nanosheet $T^1C_4C_8(S)[p,q]$ the topological indices taken into consideration consistently provide measures of structural complexity. In terms of the parameters p and q, the numerical analysis reveals a systematic increase in index values that reflects the rise in interaction density and structural connectivity. By obtaining closed-form expressions for several variations of Van, R, and S indices, the current work expands the analytical framework in contrast to previous research on degree-based topological indices. Chemical graph theory has made extensive use of these descriptors to estimate the structural behaviors and physicochemical characteristics of nanomaterials. This work offers a theoretical basis that can direct the design of energy-efficient, environmentally friendly, and sustainable nanostructures in contrast to conventional methods that depend on experiments, simulations, or laboratory trials.

4.1. Numerical analysis of Van, R, and S indices

In this part, we show the numerical calculations of the topological indices R, Van, and S for different values of the parameters p and q. We put the calculated data into tables so that we may compare them more easily. We want to find trends, relationships, and big changes in how indices behave when different parameters are set by comparing them. Our understanding of the indices predictive power and utility will improve thanks to this quantitative approach enabling us to make insightful deductions and discover new applications for them in related fields.

4.1.1. Numerical analysis of Van indices

According to Table 14, the three Van indices $\mathrm{van}_1(T^1)$, $\mathrm{van}_2(T^1)$, and $\mathrm{van}_3(T^1)$ always increase as p and q do. The carbon nanosheet networks structure becomes more intricate, and its interactions become more potent as more structural units are added. Stronger bonds and the development of a larger molecular structure are associated with larger values of p and q.

Table 14. Numerical values of $\text{van}_1(T^1)$, $\text{van}_2(T^1)$, $\text{van}_3(T^1)$, $\text{van}_r^1(T^1)$, $\text{van}_r^2(T^1)$, and $\text{van}_r^3(T^1)$ for varying p and q from 2 to 5.

p	q	$\text{van}_1(T^1)$	$\text{van}_2(T^1)$	$\text{van}_3(T^1)$	$\text{van}_r^1(T^1)$	$\text{van}_r^2(T^1)$	$\text{van}_r^3(T^1)$
2	2	16.0247	18.2716	72.0000	132.02	331.85	264.00
2	3	20.4815	23.9074	99.3333	230.03	526.66	400.00
2	4	24.9383	29.5432	126.6667	328.04	721.46	536.00
2	5	29.3951	35.1790	154.0000	426.05	916.27	672.00
3	2	20.4815	23.9074	99.3333	230.03	526.66	400.00
3	3	25.8272	30.8765	134.6667	400.04	829.46	606.00
3	4	31.1728	37.8457	170.0000	570.05	1132.27	812.00
3	5	36.5185	44.8148	205.3333	740.06	1435.07	1018.00
4	2	24.9383	29.5432	126.6667	328.04	721.46	536.00
4	3	31.1728	37.8457	170.0000	570.05	1132.27	812.00
4	4	37.4074	46.1481	213.3333	812.06	1543.07	1088.00
4	5	43.6420	54.4506	256.6667	1054.07	1953.88	1364.00
5	2	29.3951	35.1790	154.0000	426.05	916.27	672.00
5	3	36.5185	44.8148	205.3333	740.06	1435.07	1018.00
5	4	43.6420	54.4506	256.6667	1054.07	1953.88	1364.00
5	5	50.7654	64.0864	308.0000	1368.08	2472.68	1710.00

Out of all the indexes we examined, $\text{van}_3(T^1)$ grows the quickest. This is due to its greater reliance on the parameters p and q, which illustrates how the network evolves during long-distance interactions. In contrast, $\text{van}_2(T^1)$ has both direct and indirect interactions and grows steadily from there. This is a great way to discuss structural complexity without making it too easy or too difficult.

Meanwhile, $\text{van}_1(T^1)$ rises in a straight line at the same time. This gives the impression that it primarily depicts interactions that take place in tiny spaces within the nanosheet structure. Since each of the three Van indicators increases as the network expands, they are likewise positively connected. Even though these indices respond differently to structural growth, they consistently exhibit the same behavior, making them dependable and consistent measures of structural complexity.

The opposite Van indices $\text{van}_r^1(T^1)$ and $\text{van}_r^2(T^1)$ likewise increase as the values of p and q do. Overgrowth or an excessive number of connections may indicate that the network has unneeded or ineffective topologies. Never forget that $\text{van}_r^2(T^1)$ always grows more quickly than $\text{van}_r^1(T^1)$. This indicates that structures that are too tangled or unbalanced are more likely to cause it to react.

However, $\text{van}_r^1(T^1)$ grows more slowly, making it simpler to identify minor issues. When both p and q are reasonable, the analysis demonstrates that the structural design reaches equilibrium. The accurate values of the Van and reverse Van indices demonstrate this. There will be more copies, however, if the values are excessively high. This demonstrates how crucial it is to monitor structural growth to ensure that it remains robust and trouble-free. When creating robust and complex nanoscale materials in the real world, Van indices are helpful. Conversely, you may be able to identify configurations that are not functioning properly with the aid of reverse Van indices. For drug design and biotechnology, this is crucial.

4.1.2. Numerical analysis of R indices

According to Table 15, the indices $r_1(T^1)$, $r_2(T^1)$, and $r_3(T^1)$ are increasing. For larger values of p and q, $R_r^1(T^1)$ and $R_r^3(T^1)$ increase. This behavior demonstrates how the structure of the carbon nanosheet becomes increasingly intricate and interconnected as the network expands. The indices $r_1(T^1)$ and $r_2(T^1)$ grow at an exceptionally high rate due to their greater reliance on connectivity and interaction intensity, making them highly susceptible to structural changes. Conversely, $r_3(T^1)$ exhibits a more moderate growth pattern, which makes it a suitable method for characterizing nanosheet structures that are neither overly simple nor overly complex.

Table 15. Numerical values of $r_1(T^1)$, $r_2(T^1)$, $r_3(T^1)$, $R_r^1(T^1)$, $R_r^2(T^1)$, and $R_r^3(T^1)$ for varying p and q from 2 to 5.

p	q	$r_1(T^1)$	$r_2(T^1)$	$r_3(T^1)$	$R_r^1(T^1)$	$R_r^2(T^1)$	$R_r^3(T^1)$
2	2	31920	46472	3320	0.3613	0.2762	5.9332
2	3	46608	62036	4968	0.6979	0.3160	8.1220
2	4	61296	77600	6616	1.0346	0.4071	10.3108
2	5	75984	93164	8264	1.3712	0.4727	12.4996
3	2	46608	62036	4968	0.6979	0.3416	8.1220
3	3	68040	92632	7448	1.0346	0.4164	10.9775
3	4	89472	123228	9928	1.3712	0.4912	13.8329
3	5	110904	153824	12408	1.7079	0.5660	16.6884
4	2	61296	77600	6616	1.0346	0.4071	10.3108
4	3	89472	123228	9928	1.3712	0.4912	13.8329
4	4	117648	168856	13240	1.7079	0.5752	17.3551
4	5	145824	214484	16552	2.0445	0.6593	20.8772
5	2	75984	93164	8264	1.3712	0.4727	12.4996
5	3	110904	153824	12408	1.7079	0.5660	16.6884
5	4	145824	214484	16552	2.0445	0.6593	20.8772
5	5	180744	275144	20696	2.3812	0.7526	25.0660

The performance of the structural design is also further revealed by the behavior of the reverse R indices. The configurations with lower $R_r^3(T^1)$ values have less redundancy and a more efficient structure, indicating that connection and complexity are perfectly balanced. Systems requiring strong interactions, such as molecular bonding and catalytic surface design, benefit from higher values of $r_1(T^1)$ and $r_2(T^1)$. In contrast, stable and simple architectures are supported by the controlled growth of $r_3(T^1)$.

4.1.3. Numerical analysis of S indices

Table 16 lists the values of $S_1(T^1)$, $S_2(T^1)$, and $S_3(T^1)$. Both p and q undergo distinct changes as they grow. In the carbon nanosheet network, these indices demonstrate the strength of the connections and the needlessness of the structures. $S_1(T^1)$ and $S_2(T^1)$ grow rapidly as p and q increase. This indicates that the structure is more interconnected and the molecules are interacting strongly.

Table 16. Numerical values of $s_1(T^1)$, $s_2(T^1)$, and $s_3(T^1)$ for varying p and q from 2 to 5.

p	q	$s_1(T^1)$	$s_2(T^1)$	$s_3(T^1)$
2	2	3400	9096	1254
2	3	6396	15242	2030
2	4	9392	21388	2806
2	5	12388	27534	3582
3	2	6396	15242	2030
3	3	11984	25276	3238
3	4	17572	35310	4446
3	5	23160	45344	5654
4	2	9392	21388	2806
4	3	17572	35310	4446
4	4	25752	49232	6086
4	5	33932	63154	7726
5	2	12388	27534	3582
5	3	23160	45344	5654
5	4	33932	63154	7726
5	5	44704	80964	9798

On the other hand, $S_3(T^1)$ has a less steep development path that improves its ability to capture a small number of interactions inside the nanosheet framework. By observing how the reverse indices function, we can also gain a great deal of insight into how well the network architecture functions. The structures are more effective and contain fewer extras if these reverse indices are smaller. The nodes may be too close to one another though if the levels are excessively high. Connectivity patterns and structural complexity are quantified by the $S_3(T^1)$ index. Stronger possible molecular interactions are implied by denser vertex interconnections, which are associated with higher $S_3(T^1)$ values according to established chemical graph theory. When strong interactions are needed, material engineering works best when $S_1(T^1)$ and $S_2(T^1)$ are higher. For network and structural design, lower reverse index values are better because having too many connections can slow things down.

4.1.4. Overall discussion

The numerical trend shows that, with respect to the parameters p and q, the values of the considered topological indices consistently increase. A closer look, however, shows that the rate of growth becomes more noticeable at higher values of these parameters, suggesting a change in structural complexity. These differences can be understood as crucial areas where the nanolayer's structural configuration experiences notable shifts in interaction density and connectivity. Such behavior indicates possible structural transitions that may affect conductivity, stability, and energy transport properties even though no direct physical phase transition is experimentally confirmed in this study. As a result, the identified parameter ranges offer a theoretical foundation for additional experimental and computational research into phase-transition-like behavior in nanocarbon systems.

4.2. Graphical examination of Van, reverse Van, R, reverse R, and S indices

The three dimensional surface plots show how the degree-based topological indices of the nanosheet $T^1C_4C_8(S)[p,q]$ change when the structural parameters p and q change. These graphs give a clear picture of how each index grows, how symmetric it is, and how sensitive it is as the nanosheet gets bigger.

4.2.1. Van and reverse Van indices

The first, second, and third Van indices, V^1, V^2, and V^3, change over time, as shown in Figures 2–4. The surface that corresponds to the first Van index, V^1 Figure 2, has a structure that is almost flat and symmetrical. This means that it depends on the parameters p and q in a linear way. This shows that all of the vertex degrees in the nanosheet topology are the same. The second and third Van indices, V^2 and V^3, are not the same. As p and q get bigger, the curves get more dramatic and grow faster, as shown in Figures 3 and 4. In other words, as the nanosheet gets bigger, interactions with higher degrees have a bigger effect. The reverse Van indices V_r^1, V_r^2, and V_r^3 are shown in Figures 5–7. These surfaces remain symmetrical with respect to both parameters, yet their growth is somewhat more gradual than the corresponding Van indices. The moderated trend in the reverse Van indices shows that contributions from inverse degrees make highly connected vertices less important. This makes the structure clearer.

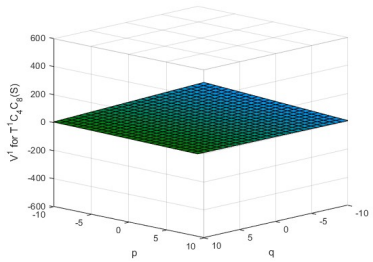

Figure 2. Graphical representation of the first Van index V^1 for the nanosheet $T^1C_4C_8(S)[p,q]$.

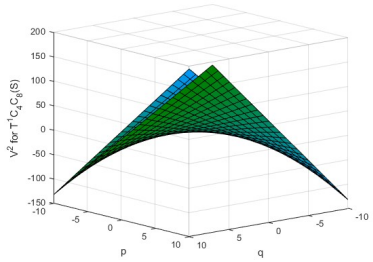

Figure 3. Graphical representation of the second Van index V^2 for the nanosheet $T^1C_4C_8(S)[p,q]$.

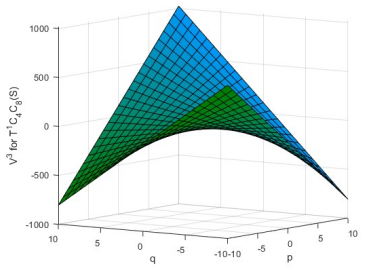

Figure 4. Graphical representation of the third Van index V^3 for the nanosheet $T^1C_4C_8(S)[p, q]$.

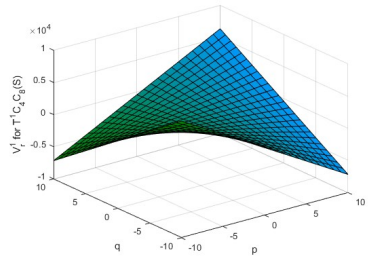

Figure 5. Graphical representation of the first reverse Van index V_r^1 for the nanosheet $T^1C_4C_8(S)[p, q]$.

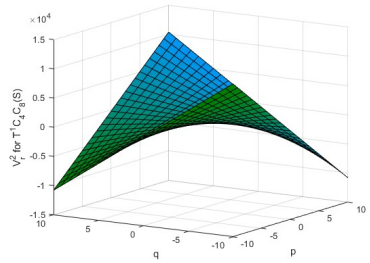

Figure 6. Graphical representation of the second reverse Van index V_r^2 for the nanosheet $T^1C_4C_8(S)[p, q]$.

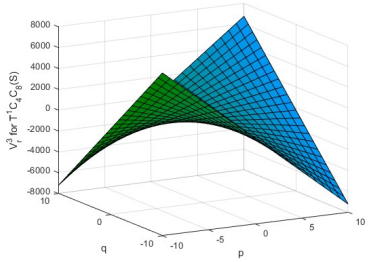

Figure 7. Graphical representation of the third reverse Van index V_r^3 for the nanosheet $T^1C_4C_8(S)[p, q]$.

4.2.2. R and reverse R indices

Figures 8–10 show the first, second, and third r indices, R^1, R^2, and R^3. All three graphs show a curved surface that slowly rises as the values of p and q go up. This steady rise shows how important it is to touch the edges. The third R index, R^3 Figure 10, shows the biggest difference in these. In other words, it reacts more strongly when the nanosheet's size and how it connects to other things change. The reverse R indices R_r^1, R_r^2, and R_r^3 are shown in the Figures 11–13. When you look at the first reverse R index, R_r^1, it looks like a line. The reverse R indices in Figures 12 and 13 are of a higher order and make things a little more curved, but not as much as the other figures. This flattening effect shows that reverse R indices can help keep things from growing too large. This makes them useful for checking the stability of structures and making comparisons.

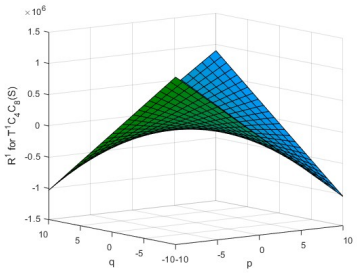

Figure 8. Graphical representation of the first r index R^1 for the nanosheet $T^1C_4C_8(S)[p, q]$.

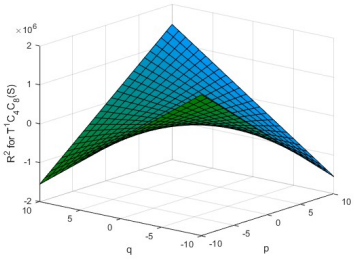

Figure 9. Graphical representation of the second r index R^2 for the nanosheet $T^1C_4C_8(S)[p, q]$.

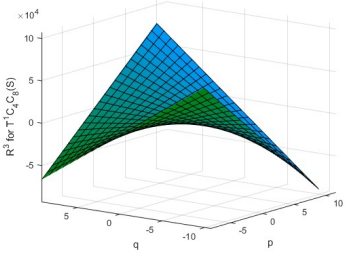

Figure 10. Graphical representation of the third r index R^3 for the nanosheet $T^1C_4C_8(S)[p, q]$.

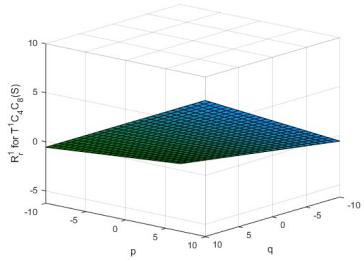

Figure 11. Graphical representation of the first reverse R index R_r^1 for the nanosheet $T^1C_4C_8(S)[p, q]$.

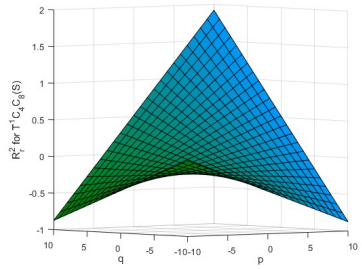

Figure 12. Graphical representation of the second reverse R index R_r^2 for the nanosheet $T^1C_4C_8(S)[p, q]$.

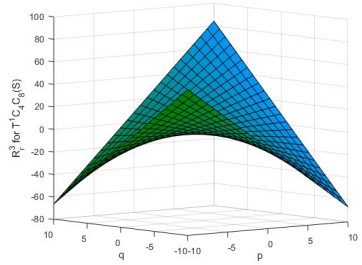

Figure 13. Graphical representation of the third reverse R index R_r^3 for the nanosheet $T^1C_4C_8(S)[p, q]$.

4.2.3. S indices

Figures 14–16 show the three-dimensional plots of the first, second, and third S indices, S^1, S^2, and S^3. These surfaces exhibit significant nonlinear growth as the values of p and q increase, characterized by distinctly elevated peaks. The symmetry seen in all s indices plots shows that the nanosheet structure is expanding evenly. Also, the fact that the slope gets steeper from S^1 to S^3 shows how higher-order degree contributions add up. The third S index, S^3 in Figure 16, is the most sensitive, which shows that it is very good at capturing changes in structural complexity and connectivity.

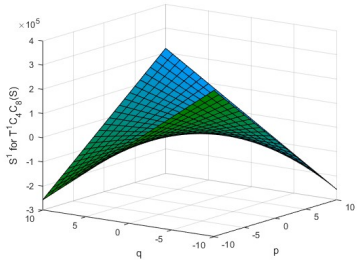

Figure 14. Graphical representation of the first s index S^1 for the nanosheet $T^1C_4C_8(S)[p,q]$.

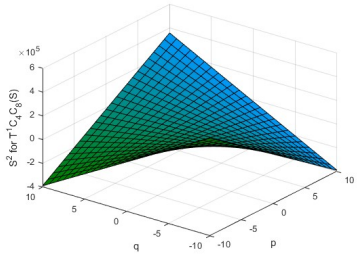

Figure 15. Graphical representation of the second s index S^2 for the nanosheet $T^1C_4C_8(S)[p,q]$.

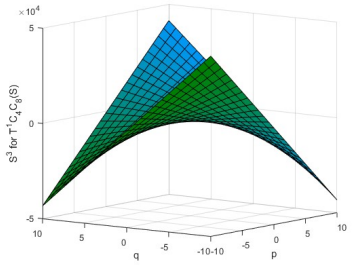

Figure 16. Graphical representation of the third s index S^3 for the nanosheet $T^1C_4C_8(S)[p,q]$.

4.2.4. Overall discussion

The graphical analysis show that, for the most part, all of the indices steadily rise as the values of p and q change. This means that the nanosheet $T^1C_4C_8(S)[p,q]$ is always getting larger. Lower-order indices move in a straight line or in a way that is mostly straight. On the other hand, higher-order indices seem to curve and grow quickly, which means they are more likely to expand structurally. The other indices, on the other hand, show surfaces that are smoother and more level. This gives us more information about how strong and balanced the nanosheet topology is. The graphs completely support the analytical formulas that were made, and they show that the proposed indices do a good job of defining nanosheet configurations. Higher order indices depend a lot on how a material is made, so they might be useful for QSAR/QSPR modeling and for learning about the nanoscale physical and chemical properties.

5. Conclusions

This research thoroughly examined the Van, R, and S topological indices of carbon nanosheet $T^1C_4C_8(S)[p,q]$. The results for a range of parametric values are presented in tables and figures, showing that they are consistent and reliably describe the physicochemical properties of the nanosheet. Future applications of advanced nanotechnology and the production of materials may benefit from the increased use of these indices particularly for two-dimensional nanostructures rather than only one-dimensional systems. To further advance this study, interested readers could concentrate on expanding the current framework to include sophisticated topological descriptors and entropy-based modeling for sustainable nanomaterials. The development of optimized materials for green energy applications and environmentally sustainable technologies may be greatly aided by such research.

The suggested graph-theoretical framework provides a mathematical way to examine and enhance network structures, which can help decision-makers, engineers, and legislators involved in the field of sustainable materials and energy-efficient systems, to choose effective configurations to reduce energy use and environmental impact. Additionally, decision-makers can assess structural properties quantitatively by using topological indices like Van, R, and S, which facilitate better-informed and data-driven choices. The results of this study have important social and practical ramifications as well for environment preservation and sustainable development. The suggested network can be used to optimize nanomaterials, design energy-efficient networks, and lower carbon emissions through better structural arrangements. Practically speaking, this framework can be applied to smart grids, renewable energy systems, and environment-friendly material engineering. It offers a basis for combining technological solutions with mathematical findings to tackle today's environmental and energy problems.

Author contributions

Jun Yang: Analysis, Review, Software, Funding Acquisition; Hifza Iqbal: Visualization, Supervision, Investigation, Editing, Conceptualization, Software, Methodology; Muhammad Akmal: Computations, Writing–Original Draft, Validation, Data Curation; Muhammad Akhtar Tarar: Supervision, Investigation, Analysis Tools, Editing. All authors have read and agreed to the published version of the manuscript.

Use of Generative-AI tools declaration

The authors declare they have not used Artificial Intelligence (AI) tools in the creation of this article.

Acknowledgments

The authors are thankful to Chaohu University Talent Introduction and Doctoral Research Start up Fund (KYQD-2023013) for financial assistance. They also appreciate reviewers for their valuable feedback.

Conflict of interest

The authors declare no conflicts of interest.

References

1. I. Gutman, N. Trinajstić, Graph theory and molecular orbitals. Total ϕ-electron energy of alternant hydrocarbons, *Chem. Phys. Lett.*, **17** (1972), 535–538. https://doi.org/10.1016/0009-2614(72)85099-1
2. R. Todeschini, V. Consonni, *Handbook of Molecular Descriptors*, Hoboken: Wiley, 2000. https://doi.org/10.1002/9783527613106
3. H. Kubinyi, QSAR and 3D QSAR in drug design Part 1: methodology, *Drug Discov. Today*, **2** (1997), 457–467. https://doi.org/10.1016/S1359-6446(97)01079-9
4. M. Dehmer, Information-teoretic concepts for the analysis of complex networkks, *Appl. Artif. Intell.*, **22** (2008), 684–706. https://doi.org/10.1080/08839510802164101
5. A. K. Geim, Graphene: Status and Prospects, *Science*, **324** (2009), 1530–1534. https://doi.org/10.1126/science.1158877
6. K. S. Novoselov, A. K. Geim, S. V. Morozov, D. Jiang, Y. Zhang, S. V. Dubonos, et al., Electric field effect in atomically thin carbon films, *Science*, **306** (2004), 666–669. https://doi.org/10.1126/science.1102896
7. H. Wiener, Structural determination of paraffin boiling points, *J. Amer. Chem. Soc.*, **69** (1947), 17–20. https://doi.org/10.1021/ja01193a005
8. E. Estrada, Community structure of networks, In: *The structure of complex networks: theory and applications*, Oxford: Oxford Academic, 2011, 187–213. https://doi.org/10.1093/acprof:oso/9780199591756.003.0010
9. B. Furtula, I. Gutman, S. Ediz, On difference of Zagreb indices, *Discrete Appl. Math.*, **178** (2014), 83–88. https://doi.org/10.1016/j.dam.2014.06.011
10. M. Randić, On characterization of molecular branching, *J. Amer. Chem. Soc.*, **97** (1975), 6609–6615. https://doi.org/10.1021/ja00856a001
11. S. Hayat, M. Imran, Computation of topological indices of certain networks, *Appl. Math. Comput.*, **240** (2014), 213–228. https://doi.org/10.1016/j.amc.2014.04.091
12. S. M. Sankarraman, H. Ranjan, Computing some novel closed neighborhood degreebased topological indices of graphene structures, *Biointerface Res. App.*, **13** (2023), 92. https://doi.org/10.33263/BRIAC131.092
13. S. Kausar, Q. Kiran, Y. Ali, M. Imran, Multiplicative neighborhood degree based indices of carbon nanostructures, *Chem. Pap.*, **80** (2026), 4391–4407. https://doi.org/10.1007/s11696-026-04700-0
14. V. M. Mathew, S. Naduvath, Centrality measures-based sensitivity analysis and entropy of nonzero component graphs, *Discret. Math. Algorit.*, **17** (2025), 2450043. https://doi.org/10.1142/S1793830924500435

15. S. Imran, M. K. Siddiqui, M. Imran, M. F. Nadeem, Computing Topological Indices and Polynomials for Line Graphs, *Mathematics*, **6** (2018), 137. https://doi.org/10.3390/math6080137

16. M. Imran, S. Akhter, Degree-based topological indices of double graphs and strong double graphs, *Discret. Math. Algorit.*, **9** (2017), 1750066. https://doi.org/10.1142/s1793830917500665

17. M. M. Hassan, Topological descriptors of molecular networks via reverse degree, *Polycycl. Aromat. Comp.*, **44** (2024), 6165–6187. https://doi.org/10.1080/10406638.2023.2274473

18. Z. B. Du, Z. Z. Liu, On the Estrada and Laplacian Estrada indices of graphs, *Linear Algebra Appl.*, **435** (2011), 2065–2076. https://doi.org/10.1016/j.laa.2011.03.057

19. G. Boreland, I. G. Todorov, A. Winter, Information theoretic parameters of noncommutative graphs and convex corners, *Illinois J. Math.*, **66** (2022), 123–187. https://doi.org/10.1215/00192082-9799163

20. W. Gao, Z. Iqbal, M. Ishaq, A. Aslam, M. Aamir, R. Sarfraz, Topological aspects of dendrimers via distance based descriptors, *IEEE Access*, **7** (2019), 35619–35630. https://doi.org/10.1109/ACCESS.2019.2904736

21. M. Munir, W. Nazeer, A. R. Nizami, S. Rafique, S. M. Kang, M-polynomials and topological indices of titania nanotubes, *Symmetry*, **8** (2016), 117. https://doi.org/10.3390/sym8110117

22. J. B. Liu, K. Wang, X. S. Zhai, Stastical analysis and topological property of a class of fractal networks, *Fractals*, **2026** (2026), 2640001. https://doi.org/10.1142/S0218348X26400013

23. H. M. Fraz, K. Ali, M. F. Nadeem, Entropy measures of silicon nanotubes using degree based topological indices. *Phys. Scr.*, **100** (2025), 015202. https://doi.org/10.1088/1402-4896/ad94b4

24. C. C. He, S. G. Xu, J. R. Zeng, W. J. Huang, Y. Yao, Y. J. Zhao, et al., A graph-based statistical model for carbon nanostructures, *J. Chem. Phys.*, **162** (2025), 154104. https://doi.org/10.1063/5.0244219

25. J. B. Liu, M. Y. Yu, G. J. Cai, J. D. Cao, The leader-follower coherence and spectral properties of weighted recursive networks under noise disturbance, *Chaos Soliton. Fract.*, **208** (2026), 118060. https://doi.org/10.1016/j.chaos.2026.118060

26. G. F. Yu, M. K. Siddiqui, M. Hussain, N. Hussain, Z. Saddique, F. G. Petros, On topological indices and entropy measures of beryllonitrene network via logarithmic regression model, *Sci. Rep.*, **14** (2024), 7187. https://doi.org/10.1038/s41598-024-57601-1

27. M. Akmal, H. Iqbal, M. A. Tarar, M. F. Hanif, Exploring structural complexity through entropy in rectangular bilayer germanium phosphide for sustainable innovations, *Chem. Pap.*, **79** (2025), 5517–5532. https://doi.org/10.1007/s11696-025-04142-0

28. M. Akmal, H. Iqbal, M. A. Tarar, M. F. Hanif, Entropy analysis of rhombohedral bilayer germanium phosphide for sustainable material development, *Chem. Pap.*, **79** (2025), 3679–3694. https://doi.org/10.1007/s11696-025-04023-6

29. K. V. Lakshmi, N. Parvathi, Topological indices relating some nanostructures, *Materials Today: Proceedings*, **68** (2022), 2382–2386. https://doi.org/10.1016/j.matpr.2022.09.106

30. S. Hayat, J. B. Liu, Comparative analysis of temperature-based graphical indices for correlating the total π-electron energy of benzenoid hydrocarbons, *Int. J. Mod. Phys. B*, **39** (2025), 2550047. https://doi.org/10.1142/S021797922550047X

31. S. Ali, M. K. Jamil, Exchange property in double edge resolving partition sets and its use in city development, *Spectrum of Decision Making and Applications*, **1** (2024), 84–98. https://doi.org/10.31181/sdmap1120246

32. S. Hayat, M. A. Khan, A. Khan, H. Jamil, M. Y. H. Malik, Extremal hyper-Zagreb index of trees of given segments with applications to regression modeling in QSPR studies, *Alex. Eng. J.*, **80** (2023), 259–268. https://doi.org/10.1016/j.aej.2023.08.051

33. S. Hayat, M. Arshad, A. Khan, Graphs with given connectivity and their minimum Sombor index having applications to QSPR studies of monocarboxylic acids, *Heliyon*, **10** (2024), e23392. https://doi.org/10.1016/j.heliyon.2023.e23392

34. M. Azeem, M. K. Jamil, On the anticancer drug structures and their locating numbers, *Spectrum of Operational Research*, **1** (2024), 44–63. https://doi.org/10.31181/sor1120245

35. S. Iqbal, H. Iqbal, M. A. Tarar, M. F. Hanif, O. A. Fiidow, Evaluation of antiarrhythmia drug through QSPR modeling and multi criteria decision analysis, *Sci. Rep.*, **15** (2025), 29216. https://doi.org/10.1038/s41598-025-14892-2

36. M. Azeem, M. K. Jamil, Constant partition dimension of different anticancer drug structures, *Spectrum of Decision Making and Applications*, **1** (2024), 64–83. https://doi.org/10.31181/sdmap1120245

37. A. Arif, S. Hayat, A. Khan, On irregularity indices and main eigenvalues of graphs and their applicability, *J. Appl. Math. Comput.*, **69** (2023), 2549–2571. https://doi.org/10.1007/s12190-023-01845-z

38. J. B. Liu, L. Guan, J. D. Cao, Property analysis and coherence dynamics for tree-symmetric networks with noise disturbance, *J. Complex Netw.*, **12** (2024), cnae029. https://doi.org/10.1093/comnet/cnae029

39. S. Ediz, M. Semiz, On Van degrees of vertices and van indices of graphs, *Mathematics and Computer Science*, **2** (2017), 35–38. https://doi.org/10.11648/j.mcs.20170204.11

AIMS Press